Structure and Ionic-Transport Properties of Lithium-Containing Garnets $Li_3Ln_3Te_2O_{12}$ (Ln = Y, Pr, Nd, Sm−Lu)

Michael P. O'Callaghan,[†] Danny R. Lynham,[†] Edmund J. Cussen,*[,†] and George Z. Chen[‡]

The School of Chemistry and The School of Chemical, Environmental and Mining Engineering, The University of Nottingham, Nottingham, United Kingdom NG7 2RD

Received April 28, 2006. Revised Manuscript Received July 23, 2006

Lithium-containing compounds of the formula $Li_3Ln_3Te_2O_{12}$ (Ln = Y, Pr, Nd, Sm−Lu) have been prepared by solid-state ceramic methods at temperatures up to 900 °C. Rietveld refinement against X-ray and neutron powder diffraction data show that these phases adopt the garnet structure (space group $Ia\bar{3}d$) with lattice parameters in the range 12.15970(14) Å ($Li_3Lu_3Te_2O_{12}$) to 12.61596(7) Å ($Li_3Pr_3Te_2O_{12}$). The Ln^{3+} and Te^{6+} cations occupy the 8-fold and octahedrally coordinated sites, and Li^+ is accommodated exclusively in the tetrahedral sites commonly occupied in the garnet structure. Neutron diffraction data collected from $Li_3Nd_3Te_2O_{12}$ at 300 and 600 °C show that the lithium coordination does not change over this temperature range. Impedance spectroscopy measurements indicate that $Li_3Nd_3Te_2O_{12}$ shows minimal Li^+ mobility with an activation energy of 1.22(15) eV, resulting in a maximum observed conductivity of $\sigma \approx 1 \times 10^{-5}$ S cm^{-1} at 600 °C.

Introduction

The search for higher-density power sources for use in portable electronic devices has led to the emergence of Li-ion batteries as the leading technology in this area.[1] This is due to a number of attractive features of lithium batteries, such as high energy density, high cycling stability, and ease of miniaturization. However, further applications[2] for this technology could be realized by increasing the gravimetric power density and moving away from the polymer electrolytes,[3] which currently have applications in this role. Replacing current technology with an all-solid-state battery could lead to substantial improvements in high-temperature operation, mechanical strength, toxicity, and environmental impact on disposal. In crystalline solids, the highest Li^+ conductivities of $\sim 1 \times 10^{-3}$ S cm^{-1} at room temperature have been realized in a number of systems,[4,5] but problems of (electro)-chemical stability mean that these high-conductivity phases are not suitable for use in rechargeable lithium batteries. Recent research has identified a series of Ta^{5+}- and Nb^{5+}-based garnets as promising lithium-ion conductors.[6,7] The conductivity of these garnet phases rivals those of the most conductive crystalline phases and, most importantly, these garnets are stable to metallic lithium, moisture, air, and common electrode materials.[8]

The well-known garnet structure has the general formula $A_3B_2C_3O_{12}$, where *A*, *B*, and *C* refer to 8-coordinate, octahedral, and tetrahedral cation sites, respectively, as illustrated in Figure 1. The identification of facile Li^+ mobility in $Li_5La_3M_2O_{12}$ (M = Nb, Ta) has led to the study of a number of related phases,[7,9] although the structure of these compounds has been controversial despite a number of X-ray diffraction studies.[10−12] The 8-fold coordinated site is occupied by La^{3+}; the M^{5+} cation resides on the centrosymmetric octahedral site, but the space group and position of the lithium cations were not conclusively identified by X-ray diffraction experiments. We have recently employed neutron diffraction to show that $Li_5La_3M_2O_{12}$ (M = Nb, Ta) crystallizes in the space group $Ia\bar{3}d$ and that the lithium occupies a range of sites.[13] The tetrahedral site commonly occupied in the garnet structure, 24d, is partially occupied (ca. 80%) by Li^+, with the remainder of the lithium distributed with considerable disorder in heavily distorted octahedral coordination at the 48g site with ca. 40% occupancy. The tetrahedral and octahedral sites are linked by a shared face and the simultaneous occupation of these adjacent sites leads to short Li−Li distance, as shown in Figure 1. The 48g sites are linked to one another by shared edges, and the distortion of the oxide octahedra provides a large aperture for Li^+ migration that, taken in conjunction with the observed Li^+ disorder on the 48g site, suggests that

* To whom correspondence should be addressed. E-mail: edmund.cussen@nottingham.ac.uk. Fax: 44-115-951-3563.

[†] The School of Chemistry, The University of Nottingham.

[‡] The School of Chemical, Environmental and Mining Engineering, The University of Nottingham.

(1) Tarascon, J.-M.; Armand, M. *Nature* **2001**, *414*, 359−367.
(2) Bruce, P. G. *Chem. Commun.* **1997**, 1817−1824.
(3) Christie, A. M.; Lilley, S. J.; Staunton, E.; Andreev, Y. G.; Bruce, P. G. *Nature* **2005**, *433*, 50−53.
(4) Robertson, A. D.; West, A. R.; Ritchie, A. G. *Solid State Ionics* **1997**, *104*, 1−11.
(5) Stramare, S.; Thangadurai, V.; Weppner, W. *Chem. Mater.* **2003**, *15*, 3974−3990.
(6) Thangadurai, V.; Kaack, H.; Weppner, W. J. F. *J. Am. Ceram. Soc.* **2003**, *86*, 437−440.
(7) Thangadurai, V.; Weppner, W. *Adv. Funct. Mater.* **2005**, *15*, 107−112.
(8) Thangadurai, V.; Weppner, W. *J. Power Sources* **2005**, *142*, 339−344.
(9) Thangadurai, V.; Weppner, W. *J. Solid State Chem.* **2006**, *179*, 974−984.
(10) Hyooma, H.; Hayashi, K. *Mater. Res. Bull.* **1988**, *23*, 1399−1407.
(11) Mazza, D. *Mater. Lett.* **1988**, *7*, 205.
(12) Isasi, J.; Veiga, M. L.; Saez-Puche, R.; Jerez, A.; Pico, C. *J. Alloys Compd.* **1991**, *177*, 251−257.
(13) Cussen, E. J. *Chem. Commun.* **2006**, 412−413.

10.1021/cm060992t CCC: $33.50
Published on Web 08/22/2006

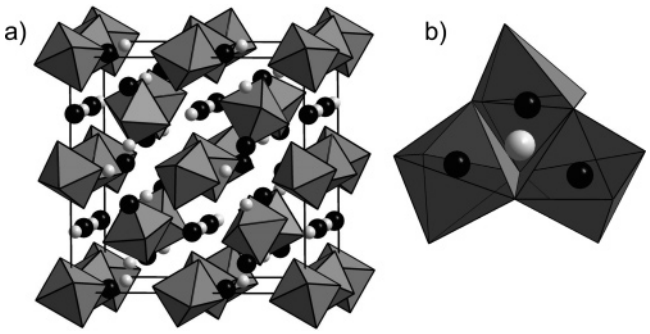

Figure 1. (a) Garnet structure of $Li_5La_3Ta_2O_{12}$ contains lithium in both tetrahedral and octahedral coordinations. Octahedra represent TeO_6 units and dark and light spheres represent lanthanum and the tetrahedrally coordinated lithium, respectively. (b) The oxide tetrahedron housing Li^+ on the 24d site (light gray) shares each face with an oxide octahedron, accommodating additional Li^+ on the 48g site (dark gray).

the LiO_6 units provided the high Li^+ mobility observed in the garnet structure.

To examine the role of the tetrahedrally and octahedrally coordinated Li^+ in the ionic conductivity of the garnet structure, we have decided to examine the compounds $Li_3Ln_3Te_2O_{12}$. Compounds from this series were first synthesized in 1968, when the lattice constants of these phases were reported,[14] but have not been structurally characterized. These compositions contain a lithium concentration that is reduced to a level such that Li^+ can be accommodated exclusively on the tetrahedral sites in the structure. The lanthanide contraction was anticipated to lead to a large variability in unit-cell size that would allow examination of the effect of chemical pressure on the relative stabilities of the different lithium sites in the garnet structure. Here, we report the crystal structures of these phases for the first time and show that the absence of octahedrally coordinated lithium has a profound effect on the transport properties of these important materials.

Experimental

Polycrystalline samples of $Li_3Ln_3Te_2O_{12}$ were prepared via typical ceramic methods: stoichiometric quantities of lithium carbonate, dried lanthanide oxide, and tellurium(IV) oxide were ground, pressed into pellets, heated in air from room temperature to 700 °C at 1 °C min^{-1} in an open alumina crucible, and held at this temperature for 6 h. The pellets were then removed from the furnace, reground, heated from 700 to 850 °C at 2.5 °C min^{-1}, and held at this temperature for 10 h. The synthesis of $Li_3Y_3Te_2O_{12}$ required the addition of 2.6% excess Li_2CO_3. In every case, these preparations were readily reproduced with no evidence of impurity phases. The progress of the reactions was monitored by X-ray powder diffraction, and in every case, the reactions had proceeded to completion, yielding a single-phase product. X-ray diffraction data suitable for Rietveld refinement were collected from the resulting materials in the range $12° \le 2\theta \le 80°$ using a Philips Xpert diffractometer operating using Cu Kα radiation.

Larger samples of some of these phases were synthesized for use in neutron diffraction experiments. Because of the large absorption cross section of ^6Li, these samples were prepared using isotopically enhanced $^7Li_2CO_3$ ($^7Li \ge 99\%$, $b_{len} = -2.22$ fm) which also increased the scattering contrast between lithium and the other nuclei. Neutron powder diffraction data were collected from a known volume of approximately 6 g of sample contained in a cylindrical vanadium can. A single sample was studied using the constant wavelength instrument D2B at the Institut Laue−Langevin, Grenoble, but the majority of data sets were collected using the Polaris diffractometer at the ISIS facility, Rutherford Appleton Laboratories. This instrument employs three detector banks to collect data in the range $0.8\ Å \le d \le 8.0\ Å$. The resulting data were corrected for absorption using the CORRECT routine within the GENIE neutron diffraction program. Rietveld refinements[15] were carried out against all three histograms simultaneously by means of the GSAS suite of programs.[16] The peak shape of the time-of-flight instrument was described using a convolution of exponential and pseudo-Voigt functions and an absorption correction was refined. The peak shape of both constant wavelength neutron and X-ray powder diffraction instruments was modeled using a pseudo-Voigt function.

Transport measurements were carried out on freshly prepared, sintered pellets of $Li_3Nd_3Te_2O_{12}$ containing a natural isotopic abundance of lithium. The cylindrical pellets were typically ca. 10 mm in diameter and 3−4 mm in thickness. The impedance measurements were carried out under an atmosphere of flowing, dry air in the temperature range $25\ °C \le T \le 600\ °C$ using platinum wires and paste to provide the electrical contact to the pellet. The platinum coating on the pellet surface acts as a blocking electrode to lithium ions and was subjected to an initial heating cycle to complete the cure before data were recorded. Collection of multiple data sets under isothermal conditions showed no time dependence of the impedance behavior of the samples after equilibriation times of 10 min. Data were collected both on heating and cooling the sample; this thermal cycle was repeated four times consecutively, using the same pellet and electrodes. Additional data sets were collected from freshly prepared pellets and electrodes, and these experiments confirmed the repeatability of the observed impedance behavior. The impedance data were collected using a driving voltage of 0.35 V over a frequency range of 1 Hz to 1 MHz. The Autolab v4.9 suite of programs was used to collect and analyze the data.

Thermogravimetric data were collected using a TA Instruments SDT Q600 thermogravimetric analyzer. The sample, ca. 30 mg, was contained in an open alumina crucible and heated to 600 °C at a rate of 5 °C min^{-1} under an atmosphere of 5% H_2 in N_2 flowing at 50 mL min^{-1}. Bond-valence analyses were carried out using literature values for bond-valence parameters.[17]

Results

Analysis of the structure of $Li_3Ln_3Te_2O_{12}$ commenced with a comparison with known garnet phases $Li_5La_3M_2O_{12}$ (M = Ta, Nb). The structures of the garnets $Li_5La_3M_2O_{12}$ have most commonly[10,18] been described in the space group $I2_13$ or $Ia\bar{3}$ and only recently have neutron diffraction experiments[13] established that the higher-symmetry space group $Ia\bar{3}d$ provides the correct description of these phases. X-ray powder diffraction data collected from $Li_3Nd_3Te_2O_{12}$ could be satisfactorily indexed in the space group $Ia\bar{3}d$, $a \approx 12.56$ Å, and a detailed examination of the diffraction patterns yielded no evidence of Bragg peaks that violated the systematic absences associated with this space group. All

(14) Kasper, H. M. *Inorg. Chem.* **1969**, *8*, 1000.
(15) Rietveld, H. M. *Acta Crystallogr.* **1969**, *2*, 65.
(16) Larson, A. C.; von Dreele, R. B. *General Structure Analysis System (GSAS)*; Los Alamos National Laboratories: Los Alamos, NM, 1990.
(17) Brese, N. E.; O'Keeffe, M. *Acta Crystallogr., Sect. B* **1991**, *47*, 192−197.
(18) Thangadurai, V.; Adams, S.; Weppner, W. *Chem. Mater.* **2004**, *16*, 2998−3006.

compounds prepared in this study yielded X-ray diffraction patterns that indicated the presence of a cubic unit cell with the same systematic absences. We note that attempts to synthesize $Li_3La_3Te_2O_{12}$ by this route did not yield any detectable quantity of garnet phase.

Preliminary structural models of $Li_3Nd_3Te_2O_{12}$ used only Nd^{3+}, Te^{6+}, and O^{2-}, placed on the special atomic positions reported for $Li_5La_3Ta_2O_{12}$, as a starting point for the Rietveld refinement and neglected the relatively small contribution of Li^+ to the total X-ray scattering power of $Li_3Nd_3Te_2O_{12}$. This simplified structural model failed to provide a satisfactory fit ($R_{wp} = 12.43$, $\chi^2 = 8.510$) to the observed data and so a difference Fourier map was calculated in order to determine the source of this mismatch between the observed and calcualted electron densities. This revealed a large positive mismatch in the difference electron density map, i.e., the observed electron density at $^1/_4$, $^7/_8$, 0 was significantly larger that the calculated electron density. Surprisingly, these coordinates corresponded to the tetrahedrally coordinated interstitial sites that are commonly occupied in the garnet structure. Fully occupying this site with lithium leads to the stoichiometry $Li_3Nd_3Te_2O_{12}$, so trial refinements were carried out with complete Li^+ occupancy of this 24d site. This led to a considerable improvement in the quality of the fit, as shown by the fit parameters $R_{wp} = 11.36$ and $\chi^2 = 7.108$. Plausible alternative lithium sites are found on the 16b and 48g positions, although the former is clearly incapable of accommodating the necessary concentration of lithium cations. A series of refinements were undertaken to investigate whether this structural model provided a uniquely satisfactory fit. Placing the lithium exclusively on the octahedral 48g site gave a refined occupancy of 1.1(2) and the fit parameters $R_{wp} = 12.31$ and $\chi^2 = 8.345$, whereas placing the lithium exclusively on the trigonal prismatic 16b site gave a refined occupancy of −1.1(2) and the fit parameters $R_{wp} = 12.36$ and $\chi^2 = 8.345$. It is clear that lithium occupancy of neither the 48g nor 16b site provides any significant improvement to the quality of fit compared to the $[Nd_3Te_2O_{12}]^{3-}$ model and that the X-ray powder diffraction data contain a significant contribution from tetrahedrally coordinated Li^+. The differences between these fits to the data are illustrated in Figure 2 and show that the lithium makes a similar contribution to most of the observed Bragg peaks below $2\theta \approx 40°$, as would be anticipated for a scattering center with a relatively large electron cloud. Analyses of the X-ray diffraction data collected from all other compounds showed a similar sensitivity to lithium coordination and unambiguously indicated the presence of LiO_4 tetrahedra in these phases. The agreement between the observed and calculated diffraction patterns was reasonable for all phases in the series, as illustrated by the data with the highest value of fit parameters ($Li_3Yb_3Te_2O_{12}$) shown in Figure 3.

In the case of $Li_3Ln_3Te_2O_{12}$ (*Ln* = Sm, Eu, Dy, Er, and Tm), it was found that the displacement parameters refined to negative values. The magnitude of the value was highly dependent on sample mounting conditions, indicating that surface roughness, combined with strong absorption, was leading to the refinement of the displacement parameters to spurious values in these compounds. Therefore, these data were analyzed by fixing the temperature factors at physically

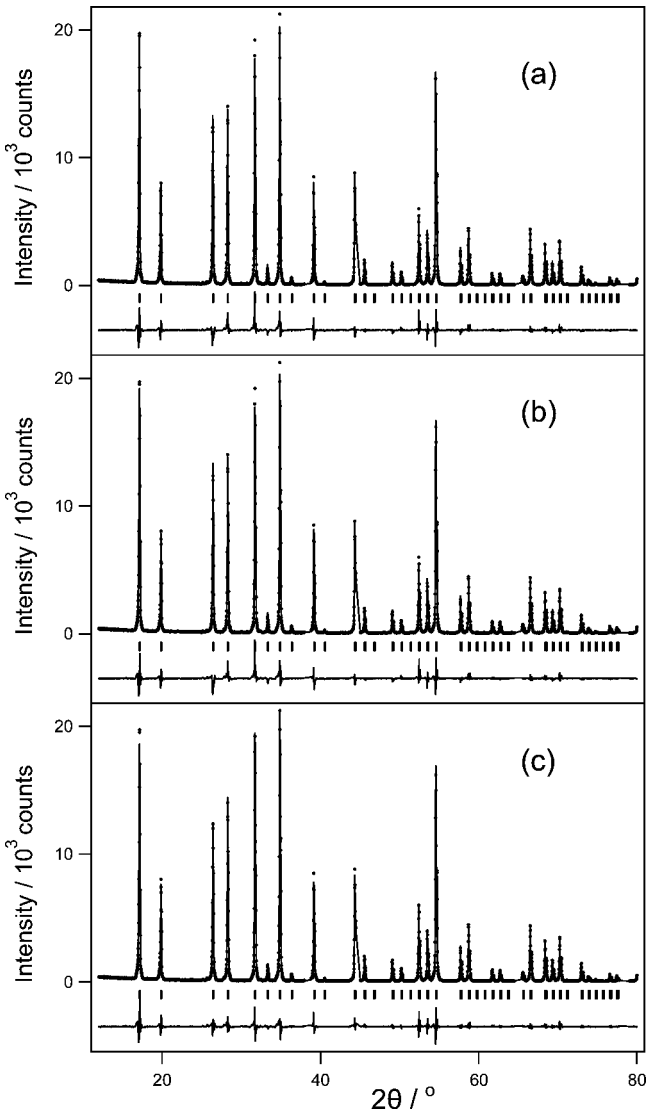

Figure 2. Observed X-ray diffraction patterns for $Li_3Nd_3Te_2O_{12}$. The solid lines represent fits obtained using different structural models: (a) $[Nd_3Te_2O_{12}]^{3-}$, (b) $Li_xNd_3Te_2O_{12}$ with unconstrained refinement of the lithium occupancy of the 48g octahedrally-coordinated site, and (c) $Li_3Nd_3Te_2O_{12}$ with all lithium on the 24g tetrahedrally-coordinated site. Excluded regions were contaminated with Bragg peaks from the aluminum sample holder.

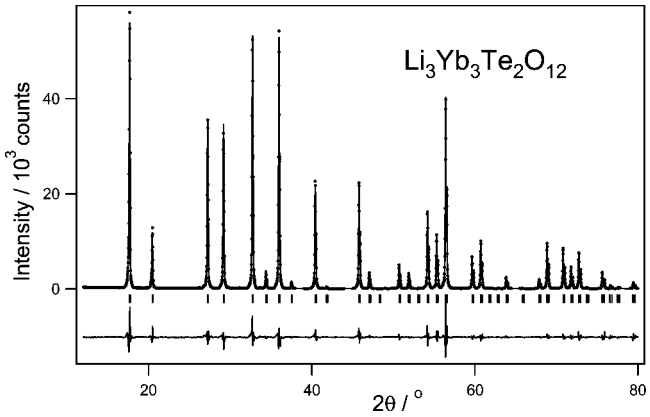

Figure 3. Observed (dots), calculated (top line), and difference (bottom line) X-ray powder diffraction patterns of $Li_3Yb_3Te_2O_{12}$. Excluded regions were contaminated with Bragg peaks from the aluminum sample holder.

reasonable values and refining the surface roughness absorption correction.

Because of the dominance of the X-ray diffraction data by the lanthanide and tellurium cations, neutron diffraction was employed to provide increased accuracy and precision in the determination of the lithium and oxide positions. Diffraction data were collected at room temperature from $Li_3Ln_3Te_2O_{12}$ (Ln = Pr, Nd, Tb, Y, and Lu) using Polaris and from $Li_3Ho_3Te_2O_{12}$ using D2B. These data were fitted using the structural model derived from the X-ray diffraction data as a starting point for the structural refinements. In every case, the refinements proceeded rapidly to convergence and provided an excellent match with the observed intensity. In order to probe the sensitivity of the neutron diffraction experiments to the position of Li^+ in the unit cell, we carried out a trial refinement in which the lithium occupancies of the tetrahedral site (24d), octahedral site (48g), and trigonal prismatic sites (16b) were independently refined, i.e., no constraint was applied to the bulk stoichiometry. This refinement against the data collected from $Li_3Nd_3Te_2O_{12}$ led to the fit parameters $R_{wp} = 2.65$ and $\chi^2 = 1.893$ and fractional occupancies of 1.045(7), 0.006(3), and 0.018(4) for the Td (tetrahedral), Oh (octahedral), and TP (trigonal prismatic) sites, respectively. The occupancies of the Oh and TP sites were subsequently set to zero, and the fractional occupancy of the tetrahedral site was fixed at unity; no further refinement of site occupancies was carried out. The application of this model to the data collected from $Li_3Lu_3Te_2O_{12}$ resulted in increased fit parameters, $R_{wp} = 5.25$ and $\chi^2 = 7.765$. Trial refinements were undertaken in space groups $Ia\bar{3}$ and $I2_13$, which are sequential subgroups that have previously been reported for garnet phases.[18] The refinement in $Ia\bar{3}$ proceeded to convergence using isotropic displacement parameters to give the fit parameters $R_{wp} = 5.26$ and $\chi^2 = 7.789$. The use of anisotropic displacement parameters gave a negligible improvement in the quality of fit ($R_{wp} = 5.25$, $\chi^2 = 7.758$) and destabilized the refinement to such an extent that it failed to converge. Reducing the symmetry further to $I2_13$ gave no improvement in the quality of fit and destabilized the refinement to such an extent that it was not possible to refine all of the atomic positions simultaneously. This thorough testing of possible lithium distribution over possible coordination sites and distortions of the garnet structure failed to provide any improvement over the $Ia\bar{3}d$ model containing Li^+ exclusively on the tetrahedral sites. The final fit obtained using this model is shown in Figure 4.

Neutron diffraction data collected using Polaris were analyzed using a total of 46 variables: 13 anisotropic displacement parameters, 3 positional parameters, 18 background parameters, 3 absorption correction parameters, 3 histogram scale factors, 5 diffractometer coefficients, and 1 lattice parameter. The data collected from $Li_3Ho_3Te_2O_{12}$ were analyzed using the same structural model. Figure 4 shows representative fits to the data collected from $Li_3Nd_3Te_2O_{12}$ and $Li_3Lu_3Te_2O_{12}$. In cases where neutron diffraction data were not available, i.e., $Li_3Ln_3Te_2O_{12}$ (Ln = Sm, Eu, Gd, Dy, Tm, Yb), the X-ray diffraction data were analyzed using a similar structural model to that described above, i.e., with a fully occupied tetrahedrally coordinated lithium site, but

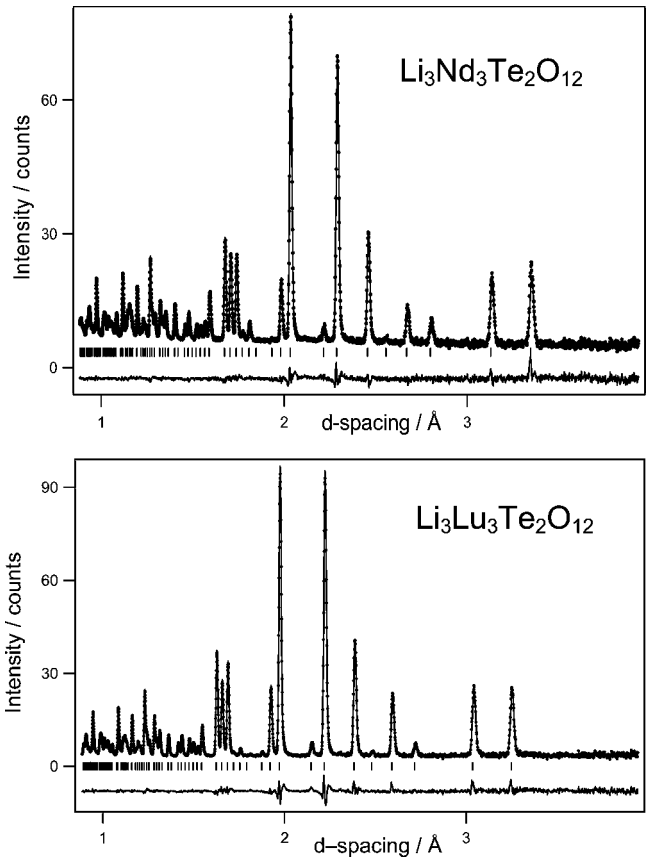

Figure 4. Observed (dots), calculated (top line), and difference (bottom line) neutron diffraction profiles collected from (top graph) $Li_3Nd_3Te_2O_{12}$ and (bottom graph) $Li_3Lu_3Te_2O_{12}$ at room temperature.

with isotropic displacement parameters. The refinement details and structural parameters for all compounds are collected in Table 1, the displacement parameters are listed in Table 2, and selected interatomic distances are shown in Table 3.

Additional neutron diffraction data sets were collected from $Li_3Nd_3Te_2O_{12}$ at 300 and 600 °C in order to probe the temperature dependence of the structure and especially the lithium coordination and disorder. An unconstrained refinement of the occupancies of the tetrahedral and octahedral sites in the structure resulted in respective occupancies of 1.028(6) and −0.003(3) at 300 °C and 1.044(4) and −0.002(2) at 600 °C, indicating that the lithium is accommodated exclusively on the tetrahedral sites between room temperature and 600 °C. The analysis of these data sets was therefore carried out using the same structural model as that employed in the refinement of the room-temperature structures. The anisotropic displacement parameters showed the largely isotropic increase in lithium scattering volume expected on heating a crystalline, well-ordered phase with no evidence of static disorder.

Impedance data collected at room temperature from $Li_3Nd_3Te_2O_{12}$ were characteristic of a highly resistive material and tested the detection limits of the instrument. On heating the sample, the impedance decreases and at temperatures of ca. 400 °C, a plot of the impedance in the complex plane takes on the well-defined shape shown in Figure 5, which shows the low-frequency tail characteristic of ionic conduction using blocking electrodes. It was not possible to

Table 1. Fit Parameters and Structural Information for $Li_3Ln_3Te_2O_{12}$ Derived from Rietveld Refinement Against X-ray or Neutron Powder Diffraction (data collected at room temperature unless otherwise stated)[a]

							$100U_{eq}$			
compd	a_o (Å)	R_{wp}	χ^2	O_x	O_y	O_z	Ln	Te	Li	O
$Li_3Pr_3Te_2O_{12}$[b]	12.61596(7)	2.69	3.25	0.27735(2)	0.10768(2)	0.20078(2)	0.60	0.43	0.95	0.68
$Li_3Nd_3Te_2O_{12}$[b]	12.56253(9)	1.71	1.905	0.27739(2)	0.10746(2)	0.20006(3)	0.54	0.57	1.01	0.75
$Li_3Sm_3Te_2O_{12}$[c]	12.4601(1)	9.08	11.72	0.2778(5)	0.1067(4)	0.1986(5)	1.0	1.0	1.0	1.0
$Li_3Eu_3Te_2O_{12}$[c]	12.4197(2)	8.35	10.97	0.2794(5)	0.1056(4)	0.1998(4)	1.0	1.0	1.0	1.0
$Li_3Gd_3Te_2O_{12}$[c]	12.3792(1)	12.19	9.03	0.2779(4)	0.1042(4)	0.1970(4)	0.38(5)	0.10(6)	2.5	0.0(2)
$Li_3Tb_3Te_2O_{12}$[b]	12.35578(9)	2.63	3.99	0.27658(2)	0.10546(2)	0.19819(2)	0.43	0.43	0.84	0.60
$Li_3Dy_3Te_2O_{12}$[c]	12.3008(1)	12.74	10.52	0.2768(5)	0.1052(5)	0.1975(4)	1.0	1.0	1.0	1.0
$Li_3Ho_3Te_2O_{12}$[b]	12.27028(6)	4.51	0.7040	0.27630(7)	0.10487(7)	0.19748(7)	0.35	0.49	1.09	0.77
$Li_3Y_3Te_2O_{12}$[b]	12.27982(9)	3.55	8.298	0.27634(2)	0.10469(2)	0.19726(2)	0.56	0.46	0.87	0.62
$Li_3Er_3Te_2O_{12}$[c]	12.22712(9)	10.14	13.54	0.2764(4)	0.1052(4)	0.1973(4)	1.0	1.0	1.0	1.0
$Li_3Tm_3Te_2O_{12}$[c]	12.2092(2)	7.09	24.72	0.2740(5)	0.1044(4)	0.1986(4)	1.0	1.0	1.0	1.0
$Li_3Yb_3Te_2O_{12}$[c]	12.16184(11)	12.96	21.69	0.2784(4)	0.1029(4)	0.1970(5)	0.22(5)	0.36(6)	1.0	0.3(2)
$Li_3Lu_3Te_2O_{12}$[b]	12.15970(14)	5.25	7.765	0.27598(4)	0.10364(4)	0.19600(4)	0.76	1.12	0.93	0.76
$Li_3Nd_3Te_2O_{12}$ 300 °C[b]	12.59860(9)	1.44	2.114	0.27713(2)	0.10761(2)	0.20038(3)	0.89	0.80	1.60	1.19
$Li_3Nd_3Te_2O_{12}$ 600 °C[b]	12.63582(9)	1.26	1.035	0.27681(2)	0.10785(2)	0.20079(3)	1.19	1.00	2.38	1.61

[a] Atomic coordinates: Ln 24c $^1/_8$, 0, $^1/_4$; Te 16a 0, 0, 0; Li 24d $^1/_4$, $^7/_8$, 0; O 96h *x, y, z.* [b] Refined against neutron diffraction data. [c] Refined against X-ray diffraction data.

Table 2. Anisotropic Displacement Parameters (Å^2) for $Li_3Ln_3Te_2O_{12}$ Derived from Rietveld Refinement Against Neutron Powder Diffraction (data collected at room temperature unless otherwise stated)

	Li[a]		Te[b]		Ln[c]			O					
compd	$100U_{11}$	$100U_{22}$	$100U_{11}$	$100U_{12}$	$100U_{11}$	$100U_{22}$	$100U_{23}$	$100U_{11}$	$100U_{22}$	$100U_{33}$	$100U_{12}$	$100U_{13}$	$100U_{23}$
$Li_3Pr_3Te_2O_{12}$	1.17(3)	0.51(5)	0.432(6)	−0.021(8)	0.74(2)	0.54(1)	0.04(1)	0.721(8)	0.550(8)	0.782(9)	0.064(5)	0.010(6)	−0.068(6)
$Li_3Nd_3Te_2O_{12}$	1.26(4)	0.51(7)	0.57(1)	−0.05(1)	0.68(2)	0.47(1)	0.08(1)	0.72(1)	0.69(1)	0.83(1)	0.013(8)	0.025(9)	−0.11(1)
$Li_3Tb_3Te_2O_{12}$	1.06(3)	0.41(5)	0.430(7)	−0.038(9)	0.54(2)	0.382(8)	0.005(9)	0.597(9)	0.539(9)	0.67(1)	0.023(6)	0.011(6)	−0.09(1)
$Li_3Ho_3Te_2O_{12}$	1.2(1)	1.0(3)	0.49(3)	0.00(5)	0.49(7)	0.28(3)	0.13(5)	0.82(4)	0.47(3)	1.01(5)	0.03(3)	0.17(3)	−0.03(4)
$Li_3Y_3Te_2O_{12}$	1.04(4)	0.52(6)	0.463(8)	−0.04(1)	0.63(2)	0.524(9)	−0.01(1)	0.64(1)	0.553(10)	0.68(1)	0.040(6)	0.021(7)	−0.08(1)
$Li_3Lu_3Te_2O_{12}$	1.27(6)	0.83(10)	0.76(1)	−0.03(2)	0.87(3)	0.79(2)	−0.01(2)	0.92(2)	0.85(2)	1.01(2)	0.03(1)	0.01(1)	−0.04(1)
$Li_3Nd_3Te_2O$ 300 °C	1.96(5)	0.88(8)	0.80(1)	−0.07(1)	1.02(2)	0.83(1)	0.20(1)	1.23(1)	0.96(1)	1.37(2)	0.07(1)	0.04(1)	−0.16(1)
$Li_3Nd_3Te_2O_{12}$ 600 °C	2.84(6)	1.47(10)	1.00(1)	−0.10(2)	1.22(3)	1.17(1)	0.40(2)	1.76(2)	1.16(2)	1.92(2)	0.21(1)	0.06(1)	−0.18(1)

[a] $U_{33} = U_{11}$, $U_{12} = U_{13} = U_{23} = 0$. [b] $U_{33} = U_{22} = U_{11}$, $U_{13} = U_{23} = U_{12}$. [c] $U_{33} = U_{22}$, $U_{12} = U_{13} = 0$.

Table 3. Selected Interatomic Distances (Å) and Angles (deg) Derived from Rietveld Refinement Against X-ray Or Neutron Powder Diffraction (data collected at room temperature unless otherwise stated)

compd	Li−O × 4	Te−O × 6	O−Te−O(1)	O−Te−O(2)	Ln−O(1) × 4	Ln−O(2) × 4	Ln−O−Ln
$Li_3Pr_3Te_2O_{12}$[a]	1.9362(2)	1.9309(2)	85.674(9)	94.326(9)	2.4342(2)	2.5657(2)	101.139(7)
$Li_3Nd_3Te_2O_1$[a]	1.9286(3)	1.9284(3)	85.508(13)	94.492(13)	2.4251(3)	2.5463(3)	101.352(13)
$Li_3Sm_3Te_2O_{12}$[b]	1.893(5)	1.958(5)	85.2(2)	94.8(2)	2.404(5)	2.497(6)	101.7(2)
$Li_3Eu_3Te_2O_{12}$[b]	1.876(6)	1.934(5)	86.4(3)	93.6(3)	2.405(5)	2.520(5)	101.1(2)
$Li_3Gd_3Te_2O_{12}$[b]	1.882(5)	1.951(5)	85.0(2)	95.1(2)	2.382(5)	2.476(5)	102.5(2)
$Li_3Tb_3Te_2O_{12}$[a]	1.8938(2)	1.9254(2)	84.638(11)	95.362(11)	2.3697(2)	2.4825(3)	102.439(9)
$Li_3Dy_3Te_2O_{12}$[b]	1.883(6)	1.923(6)	84.6(3)	95.4(3)	2.362(5)	2.464(5)	102.6(2)
$Li_3Ho_3Te_2O_{12}$[a]	1.8809(9)	1.9211(9)	84.33(4)	95.67(4)	2.3489(9)	2.4570(9)	102.82(3)
$Li_3Y_3Te_2O_{12}$[a]	1.8814(3)	1.9257(3)	84.289(11)	95.711(11)	2.3507(3)	2.4566(3)	102.890(10)
$Li_3Er_3Te_2O_{12}$[b]	1.879(5)	1.911(5)	84.3(2)	95.7(2)	2.344(5)	2.446(5)	102.81(18)
$Li_3Tm_3Te_2O_{12}$[b]	1.881(6)	1.908(5)	83.5(3)	96.5(3)	2.308(5)	2.455(5)	103.4(2)
$Li_3Yb_3Te_2O_{12}$[b]	1.825(5)	1.944(5)	85.2(2)	94.8(2)	2.330(5)	2.437(5)	102.7(2)
$Li_3Lu_3Te_2O_{12}$[a]	1.8625(4)	1.9231(4)	83.81(2)	96.19(2)	2.3216(4)	2.4181(5)	103.52(2)
$Li_3Nd_3Te_2O_{12}$ 300 °C[a]	1.9363(3)	1.9302(3)	85.463(13)	94.537(13)	2.4294(3)	2.5570(3)	101.328(11)
$Li_3Nd_3Te_2O_{12}$ 600 °C[a]	1.9450(3)	1.9311(3)	85.406(14)	94.594(14)	2.4336(3)	2.5685(3)	101.297(11)

[a] Refined against neutron diffraction data. [b] Refined against X-ray diffraction data.

separate the bulk and grain boundary contributions to the conductivity; a value for the total conductivity was extracted by fitting a circular arc to the high-frequency data and correcting for the dimensions of the pellet. The conductivity values extracted from multiple heating and cooling cycles are shown in an Arrhenius plot in Figure 6. Fitting each of the seven cooling and heating cycles independently to the Arrhenius equation resulted in values of the activation energy of 1.22(15) eV. Because of the difficulties of extracting accurate values for the conductivity from this highly resistive material, it is possible that these data mask a subtle change in activation energy. However, alternative analyses of these data using a model containing two activation-energy regimes failed to produce statistically significant evidence of more than one activation energy over this temperature range.

The operation of solid electrolytes often requires stability to a range of redox environments, often at elevated temperatures. To examine the stability of tellurate garnets to reducing conditions, we heated a sample of $Li_3Nd_3Te_2O_{12}$ under a flowing atmosphere of 5% H_2 and recorded the mass as a function of temperature. The material showed no significant change in mass at temperatures up to 500 °C, but then showed a rapid mass loss, as shown in Figure 7. X-ray diffraction data collected from the product indicated that reduction to Nd_2TeO_2, Nd_2O_3, Li_2O, and metallic tellurium had occurred. The observed mass loss, 82 wt %,

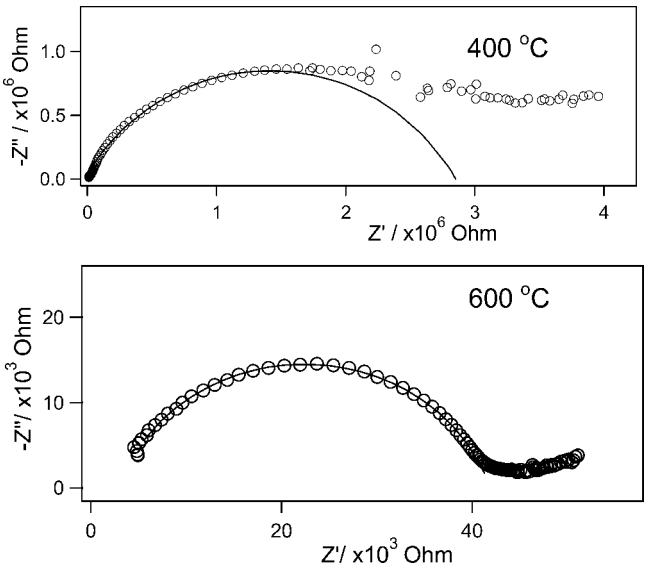

Figure 5. Complex plane impedance plots collected from $Li_3Nd_3Te_2O_{12}$ using ion-blocking electrodes at (a) 400 and (b) 600 °C show impedances varying by a factor of ca. 1×10^2 over this temperature range. The curves represent fits to the high-frequency end of the spectrum.

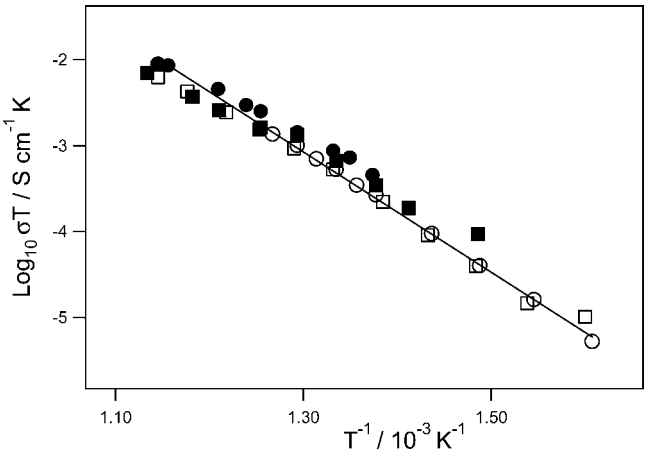

Figure 6. Arrhenius plot of the conductivity of $Li_3Nd_3Te_2O_{12}$ as a function of temperature. The initial and final temperature cycles are represented by circles and squares, respectively. Data collected on heating are shown by filled symbols, whereas data points collected on cooling are empty. The line represents a fit to the initial cooling (empty circles) data set.

is considerably greater than that expected for either of the possible limits of the reduction

$$Li_3Nd_3Te_2O_{12} \xrightarrow{H_2} {}^3/_2Li_2O + {}^3/_2Nd_2O_3 + 2Te\ [+ H_2O\uparrow]\ 89.3\ wt\ \% \quad (1)$$

$$Li_3Nd_3Te_2O_{12} \xrightarrow{H_2} {}^3/_2Li_2O + {}^1/_2Te + {}^3/_2Nd_2TeO_2\ [+ H_2O\uparrow]\ 86.6\ wt\ \% \quad (2)$$

Reductions 1 and 2 both produce elemental tellurium (m.p. 450 °C) in sufficient quantities that partial evaporation of this component from the mixture could lead to a further reduction in mass to 82 wt %. The data are not able to distinguish between the two possible reactions, but clearly show that reduction to Te^0 and lower oxidation states has occurred.

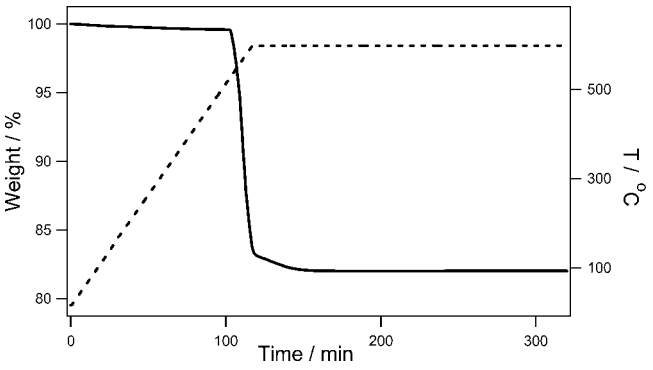

Figure 7. Variation in mass (solid line) as a function of temperature (dotted line) for $Li_3Nd_3Te_2O_{12}$ heated under a flowing atmosphere of 5% H_2 in N_2.

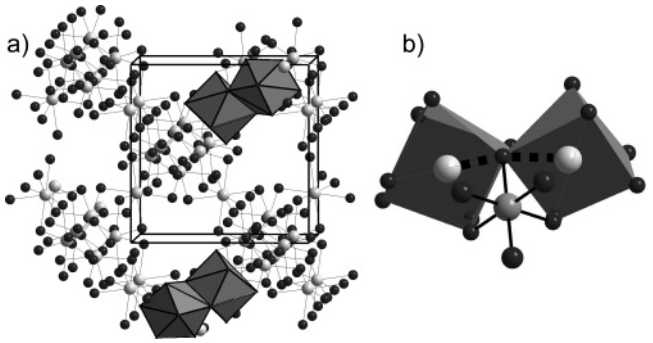

Figure 8. Edge-sharing of LnO_8 cubes in $Li_3Ln_3Te_2O_{12}$ leads to the formation of two interpenetrating body-centered lattices. One of these frameworks composed of Ln (light gray spheres) and O (dark gray spheres) is shown in (a) along with selected polyhedra to illustrate the linkages between the LnO_8 units. Tellurium is accommodated in an octahedral site (b) that shares edges with an edge-linked LnO_8 dimer. The dashed lines represent the angle that varies with the changing radius of Ln^{3+}.

Discussion

Structural refinements against laboratory X-ray powder diffraction data have shown that the compounds $Li_3Ln_3Te_2O_{12}$ adopt the garnet structure, with the tetrahedral, cubic, and octahedral sites commonly occupied in garnets accommodating Li^+, Ln^{3+}, and Te^{6+}, respectively. A surprising component of this discovery is the sensitivity of these X-ray diffraction data to the lithium cations in the presence of multiple heavy atoms. The observed intensity of diffracted X-rays varies as the square of the number of electrons; it would thus be anticipated that the contribution from Li^+ $(2\ e^-)^2$ would be negligible compared to those from Nd^{3+} $(57\ e^-)^2$ and Te^{6+} $(46\ e^-)^2$, which would dominate the observed X-ray diffraction pattern. It seems probable that this unexpected sensitivity is associated with the high symmetry of the phase; this leads to both a relatively small number of reflections (such that the problems associated with peak overlap are largely absent from these powder diffraction data) and a small number of variables in the structure. The latter prevents the contribution of lithium to the pattern from being masked by refinement of other atomic variables to spurious values. Although it seems that this accurate detection of lithium from powder X-ray data may depend on a fortuitous combination of structural features, it does suggest that Rietveld refinement against X-ray data can provide useful information on extremely weak scatterers and the contribution of these species to the X-ray diffraction profile should not be neglected. Although X-ray data provided useful

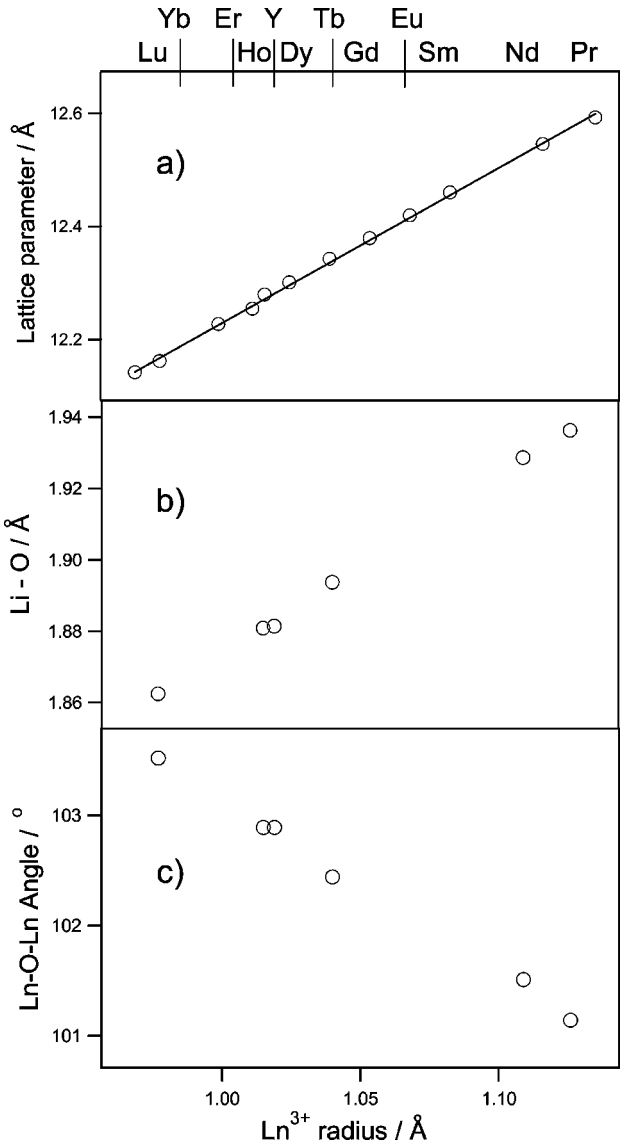

Figure 9. The variation in (a) lattice parameter, (b) lithium oxide bond length, and (c) Ln−O−Ln angle in $Li_3Ln_3Te_2O_{12}$ as a function of the radius of Ln^{3+}. The fitted line shown in (a) illustrates that this series obeys Vegard's law.

information on these garnets, the application of neutron powder diffraction improved the precision in the bond distances by at least an order of magnitude, demonstrating the power of this technique.

The large variation in lattice parameters exhibited by the series $Li_3Ln_3Te_2O_{12}$ illustrates the ability of the garnet structure to accommodate varying sizes of cations with no change in symmetry. This structure can be considered to be formed from two interpenetrating, body-centered lattices composed of edge-shared distorted LnO_8 cubes, as shown in Figure 8. Because of the resulting isotropic three-dimensional connectivity provided by the cubic symmetry, it follows that the observed lattice contraction is predominantly controlled by the reduction in lanthanide radius with increasing atomic number, as shown in Figure 9. An examination of the magnitude of the observed variation in lattice parameter shows that although the unit cell decreases in size with increasing atomic number of Ln, it does so to a lesser degree than the Ln−O bond lengths. The decrease in lattice parameter with atomic number is offset by a significant increase in the Ln−O−Ln angle, as shown in Figure 9, i.e., the structure distorts with no reduction in symmetry, in such a manner that counteracts the effect of increasing lanthanide size. The Te^{6+} cations occupy interstitial sites between LnO_8 units, so the structural adjustment in the Ln−O framework leads to a small extension in the Te−O distance as the lanthanide size is increased. However, this distance remains in the range expected for Te^{6+}; analysis of the bond lengths derived from the neutron diffraction data show a calculated valence[17] of tellurium in the range +5.78 ($Li_3Pr_3Te_2O_{12}$) to +5.90 ($Li_3Lu_3Te_2O_{12}$).

The mass loss observed on heating $Li_3Nd_3Te_2O_{12}$ under 5% H_2 is due to the reduction of this compound and is not unexpected given the relative instability of Te^{6+}. The ease of reduction of $Li_3Nd_3Te_2O_{12}$ indicates that tellurium-containing garnet phases will be unsuitable electrolytes for applications that will involve exposure to reducing conditions, such as those found in rechargeable lithium batteries. Nevertheless, the observations of the ionic conductivity in $Li_3Nd_3Te_2O_{12}$ can be combined with our knowledge of the structure and lithium environments and provide a valuable insight into the general conditions necessary for Li^+ mobility in the garnet structure.

Previous observations in the related compounds $Li_5La_3Ta_2O_{12}$ and $Li_5La_3Nb_2O_{12}$ have shown considerable ionic mobility.[6] In these compounds, the tetrahedral sites contain ca. 20% vacancies, and the remaining lithium occupies 40% of the octahedral sites with considerable positional disorder.[13] It was argued that this averaged structure sampled by the diffraction experiments did not represent the local structure but that the observed disorder was due to the existence of clusters of stoichiometries $[Li_3La_3M_2O_{12}]^{2-}$ and $[Li_6La_3M_2O_{12}]^{+}$ containing lithium exclusively in tetrahedral or octahedral coordination, respectively. This is the only interpretation of the average crystal structure that does not necessitate the presence of unacceptably short Li···Li distances; similar clustering is a feature of other crystalline, fast Li^+ conducting phases.[19]

The structures derived in the current study of $Li_3Ln_3Te_2O_{12}$ show unambiguously that the lithium is housed exclusively in the tetrahedral sites in these phases. The observation of full site occupancy in $Li_3Ln_3Te_2O_{12}$ shows that where the lithium concentration is sufficient to precisely fill the tetrahedral site, the octahedral site remains vacant. Although we were unable to prepare a garnet phase of composition $Li_3La_3Te_2O_{12}$ to compare with $Li_5La_3M_2O_{12}$ phases, the Li−O distance in $Li_3Pr_3Te_2O_{12}$, 1.9362(2) Å, is almost identical to that observed in the tetrahedrally coordinated Li^+ environment in $Li_5La_3Ta_2O_{12}$, 1.9360(4) Å, suggesting that the chemistry of these LiO_4 units should be similar in these compounds. The complete absence of mixing of lithium coordinations in $Li_3Pr_3Te_2O_{12}$ shows that the presence of vacancies on the tetrahedral site is not an inherent property of the lithium chemistry of the garnet structure and that entropic considerations alone are insufficient to introduce mixed lithium distributions in these phases. This provides

(19) Abrahams, I.; Bruce, P. G.; David, W. I. F.; West, A. R. *Acta Crystallogr., Sect. B* **1989**, *45*, 457−462.

strong support for the argument that the substantial vacancy concentration observed on both octahedral and tetrahedral lithium sites in $Li_5La_3M_2O_{12}$ arises from the cluster model previously proposed.[13]

The Li−O distance shows a regular evolution across the series from 1.9362(2) Å for $Li_3Pr_3Te_2O_{12}$ to 1.8625(4) Å for $Li_3Lu_3Te_2O_{12}$, as shown in Figure 9. These distances lead to bond valence sums of 1.124 and 1.368 valence units, respectively, suggesting that the lithium cation experiences a substantial increase in overbonding with reducing lanthanide size and that in $Li_3Lu_3Te_2O_{12}$, this tetrahedral site is considerably smaller than the optimum size. Indeed, we had anticipated that the chemical pressure applied by the substitution of Lu^{3+} could be sufficient to depopulate the tetrahedral site in favor of the vacant, heavily distorted, octahedral interstitial sites at the 48g position ($^1/_8$, ≈ 0.683, ≈ 0.567). In $Li_3Lu_3Te_2O_{12}$, this site would provide a environment with three pairs of Li−O distances, 1.929, 2.277, and 2.308 Å, resulting in a calculated bond valence of 1.00. This can be contrasted with the distances reported for $Li_5La_3Ta_2O_{12}$, where the same site is 40% occupied in a disordered manner and yields a valence of 0.81 for Li^+. These observations of such a wide range of calculated valences for both the tetrahedral and octahedral lithium positions in these garnet phases suggests that the bond-valence approach has substantial shortcomings when applied to this system and is unable to predict which of the interstitial sites provides the most favorable site for lithium cations. It is interesting to note that calculations of the bond-valence sum for a fictitious octahedrally coordinated lithium placed on the vacant 48g site of $Li_3Nd_3Te_2O_{12}$ provide a valence, 0.79, that is an excellent match to that observed (0.81) for the occupied 48g site in $Li_5La_3Ta_2O_{12}$. These observations show that analyses of the structures of lithium garnets through the empirical approach of bond-valence sums do not provide a reliable, accurate prediction of the experimentally observed structures and thus caution should be applied to the application of these metrics.

The transport properties of $Li_3Nd_3Te_2O_{12}$ are vastly different from those reported previously in related lithium garnets. The compounds $Li_5La_3Ta_2O_{12}$ and $Li_6BaLa_2Ta_2O_{12}$ show room-temperature conductivities of ca. 1.2×10^{-6} and 4.0×10^{-5} S cm^{-1}, respectively.[7] The low activation energies for conduction in these phases, ca. 0.45 eV, results in a rapid increase in conductivity with increasing temperature and values of conductivity in excess of 1×10^{-2} S cm^{-1} are observed at 300 °C, whereas $Li_3Nd_3Te_2O_{12}$ shows such a low level of conductivity at room temperature that it could not be measured accurately. The observed increase in conductivity on heating $Li_3Nd_3Te_2O_{12}$ gave more reliable results for elevated temperatures and showed that the conductivity reached a maximum value of only 1×10^{-5} S cm^{-1} at 600 °C. The linear nature of the Arrhenius plot clearly shows that the charge transport in this compound is occurring via a process that can be characterized by an activation energy of 1.22(15) eV over the observed temperature range. This value is 2−3 times greater than that reported for the more conductive phases and indicates that Li^+ mobility in $Li_3Nd_3Te_2O_{12}$ utilizes a different mechanism than the fast ion-conducting phases. Consequently, $Li_3Nd_3Te_2O_{12}$ can be considered to have relatively immobile lithium cations, as implied by the Li^+ displacement parameters. The high-temperature neutron diffraction experiments show that the lithium cations remain highly ordered on the tetrahedral sites in $Li_3Nd_3Te_2O_{12}$ at temperatures up to 600 °C and that no significant changes in the structure occur on heating.

There are several structural differences between the compounds $Li_5La_3Ta_2O_{12}$ and $Li_3Nd_3Te_2O_{12}$ that could be anticipated to influence the movement of Li^+ throughout the material. Because of the full occupancy of the Ln and Ta/Te sites, these coordination sites cannot host Li^+ cations and so will play no direct role in the Li^+ conduction pathway. Instead, Li^+ mobility must involve migration through the voids in the structure defined by the oxide sublattice. This migration path will differ between $Li_5La_3Ta_2O_{12}$ and $Li_3Nd_3Te_2O_{12}$ because of (i) changes in the lattice polarization and (ii) changes in the lithium coordination geometries and site occupation.

The change from Ta^{5+} to Te^{6+} will slightly increase the polarization of the oxide sublattice; it is thus possible that this change in metal oxidation state could lead to some adjustment in ionic conductivity. Doping studies of the Li^+ conducting perovskite phase $Li_{0.36}La_{0.55}TiO_3$ have shown that changes in cation charge and size typically cause a variation in conductivity within 1 order of magnitude, e.g., $LiSr_{1.65}Ti_{1.3}Ta_{1.7}O_9$ and $LiSr_{1.65}Zr_{1.3}Ta_{1.7}O_9$ have conductivities of 4.9×10^{-5} and 1.3×10^{-5} S cm^{-1}, respectively.[20] The relatively small change in framework polarization between $Li_5La_3Ta_2O_{12}$ and $Li_3Nd_3Te_2O_{12}$ is unlikely to be responsible for inducing the large change in transport properties between these two compounds. The behavior of $Li_{0.36}La_{0.55}TiO_3$-related phases suggests that changes in lithium coordination provide a much stronger candidate for the origin of the differences in Li^+ conductivity. Although $Li_{0.36}La_{0.55}TiO_3$ exhibits a conductivity of ca. 1×10^{-3} S cm^{-1} at room temperature, the Pr and Nd analogues have values of ca. 1×10^{-5} and 1×10^{-6} S cm^{-1} respectively.[21] This is due to the change in lithium coordination from predominantly vacant square planar sites[22] in $Li_{0.36}La_{0.55}TiO_3$ to almost fully occupying the central interstice in the Pr and Nd analogues.[21] The observation of full tetrahedral site occupancy in $Li_3Nd_3Te_2O_{12}$ compared to the occupational disorder in both tetrahedral and octahedral Li^+ sites in $Li_5La_3Ta_2O_{12}$ suggests a strong parallel with the observations in $Li_{0.36}Ln_{0.55}TiO_3$. This change in lithium coordination coupled with the introduction of disorder suggests that the mechanisms for conduction in $Li_3Nd_3Te_2O_{12}$ and $Li_5La_3Ta_2O_{12}$ would be anticipated to differ substantially, as indicated experimentally by the variation in both the overall conductivity and the activation energy.

It has previously been noted that in the fast ion-conducting phase $Li_5La_3Ta_2O_{12}$, a pathway for facile Li^+ hopping exists

(20) Sebastian, L.; Gopalkrishnan, J. *J. Mater. Chem.* **2003**, *13*, 344−441.
(21) Skakle, J. M. S.; Mather, G. C.; Morales, M.; Smith, R. I.; West, A. R. *J. Mater. Chem.* **1995**, *5*, 1807−1808.
(22) Yashima, M.; Itoh, M.; Inaguma, Y.; Morii, Y. *J. Am. Chem. Soc.* **2005**, *127*, 3491−3495.

between the edge-sharing 48g octahedral sites.[13] In $Li_3Nd_3Te_2O_{12}$, these 48g sites are unoccupied and the Li^+ is housed in the 24d site. The four faces of the LiO_4 tetrahedron in $Li_3Ln_3Te_2O_{12}$ are each shared with a vacant octahedral 48g site, so a transport mechanism can be imagined in which the first step involves migration of Li^+ from a tetrahedral site to one of the four adjacent, vacant octahedral sites. Once population of such an octahedral site has occurred, the mobility could then occur via the as of yet unknown mechanism active in $Li_5La_3M_2O_{12}$ and $Li_6BaLa_2Ta_2O_{12}$. If such a mechanism is responsible for the observed ionic conduction, the activation energy derived from $Li_3Nd_3Te_2O_{12}$, 1.2 eV, then provides an indication of the energy barrier to hopping of Li^+ from the tetrahedral site to a neighboring octahedron. It is difficult to envisage a method of providing experimental verification of such a mechanism, but we note that this is a plausible model to account for the observation of such different activated conductivity in $Li_3Nd_3Te_2O_{12}$ and $Li_5La_3Ta_2O_{12}$.

This provides the strongest evidence so far that the tetrahedral sites play no direct part in the ionic mobility in this family of lithium garnets. The proximity of the tetrahedral and octahedral sites in the structure suggests that simultaneous occupation is not possible, so population of the former necessarily reduces the number of accessible sites for Li^+ migration. This suggests that a combination of partially occupied octahedrally, and entirely vacant tetrahedrally, coordinated sites may lead to significantly enhanced ionic conductivity in this structure. However, as no phases have been characterized that contain Li^+ exclusively on the octahedral site, it may be that (partial) occupation of the tetrahedral sites is a vital ingredient in generating the population of octahedral sites necessary to optimize the transport properties of the phases.

Conclusions

The compounds $Li_3Ln_3Te_2O_{12}$ form an isostructural series containing lithium exclusively on the fully occupied tetrahedral sites of the garnet structure. Our observations in $Li_3Ln_3Te_2O_{12}$ show that the presence of mixed lithium coordination is not an inherent property of the garnet structure, that Li^+ will preferentially occupy the tetrahedral site, and that Li occupation of the octahedral site only occurs after a concentration of >3 Li^+ per formula unit is reached. They thus provide a valuable comparison to the fast lithium-ion-conducting phases based on Ta^{5+}, which contain a mixture of octahedral and tetrahedral lithium coordinations as well as vacancies on both of these sites. The transport properties of $Li_3Nd_3Te_2O_{12}$ show that the Li^+ mobility is reduced by several orders of magnitude and the activation energy is doubled compared to garnets containing Li^+ on partially occupied octahedral sites. This suggests a strategy for enhancing the transport properties in the garnet system by achieving an optimal concentration of lithium on the octahedral site while simultaneously leaving the tetrahedral site vacant. However, the variability in Li−O bond lengths observed in $Li_3Ln_3Te_2O_{12}$ suggests that the tetrahedral site will require considerable compression before Li^+ cations vacate it in preference for octahedral geometry.

Acknowledgment. We are grateful to the Royal Society for the provision of a University Research Fellowship to E.J.C., the University of Nottingham for funding, and Dr. R. Smith at Rutherford Appleton Laboratories and Dr. P. Henry at Institut Laue Langevin for assistance with the neutron scattering experiments.

CM060992T